Research Article | Vol. 26, No. 21 | 15 Oct 2018 | OPTICS EXPRESS 27894
Optics EXPRESS

Rectangular Hermite non-uniformly correlated beams and its propagation properties

JIAYI YU,[1,2] YANGJIAN CAI,[1,3,4] AND GREG GBUR[2,5]

[1]School of Physical Science and Technology & Collaborative Innovation Center of Suzhou Nano Science and Technology, Soochow University, Suzhou 215006, China
[2]Department of Physics and Optical Science, University of North Carolina at Charlotte, Charlotte, North Carolina 28223, USA
[3]Center of Light Manipulations and Applications & Shandong Provincial Key Laboratory of Optics and Photonic Device, School of Physics and Electronics, Shandong Normal University, Jinan 250014, China
[4]yangjiancai@suda.edu.cn
[5]gjgbur@uncc.edu

Abstract: We introduce a new class of non-uniformly correlated beams that are called rectangular Hermite non-uniformly correlated (RHNUC) beams, which possess rectangular symmetry in their degree of coherence. It is shown that, in free space and in turbulence, these beams possess self-focusing properties and that the position of the focus can be adjusted in 3-D space by manipulating the correlation properties of the source. Furthermore, it is demonstrated that, by choosing different mode orders and correlation lengths along two transverse directions, one creates astigmatic beams that can be designed to have a high and near-constant intensity over an extended propagation range.

1. Introduction

Much of the research in optical coherence theory has focused on studying beams of Gaussian Schell-model (GSM) form. For such beams, bothless affect by turbulence the intensity and degree of coherence (DOC) have Gaussian distributions, and the DOC is a homogeneous and isotropic function (Schell-model) [1]. Until recently, only a few papers were devoted to partially coherent beams (PCBs) with non-conventional correlations (i.e. non-Gaussian correlated), such as J_0-correlated Schell-model beams [2] and vortex-carrying partially coherent beams [3]. Investigations of such beams were limited due to the difficulty in proving that a given function is, in fact, a mathematically valid correlation function.

But in 2007, a powerful new method for designing correlation functions of scalar PCBs was introduced by Gori *et al.* [4], followed in 2009 by a more general method for vector PCBs [5], allowing a wide variety of novel PCBs to be investigated. Among the classes that have been studied since then are multi-Gaussian correlated Schell-model beams [6], Laguerre-Gaussian correlated Schell-model beams [7], Hermite-Gaussian Schell-model beams [8], and optical coherence lattices [9]. Such beams display many extraordinary and potentially beneficial properties, such as flat-topped and ring-shaped intensity profiles in the far field, self-splitting properties, and lattice-like intensity patterns that form on propagation.

In 2011, Lajunen *et al.* introduced a class of PCBs with spatially variant correlation functions (i.e. non-uniformly correlated beams) [10]. This class exhibits self-focusing and self-shifting on propagation. Higher-order non-uniformly correlated beams were introduced in 2018, and their propagation properties were also investigated [11]. Later in 2018, we extended these ideas and introduced a new infinite class of beams called Hermite non-uniformly correlated (HNUC) beams, in which both mode order and correlation length may be tuned to adjust the focal properties of the beam [12].

There are other potential benefits to developing novel PCB classes. When a laser beam

#341393 https://doi.org/10.1364/OE.26.027894
Journal © 2018 Received 2 Aug 2018; revised 19 Sep 2018; accepted 20 Sep 2018; published 9 Oct 2018

Optics EXPRESS

propagates through atmospheric turbulence, it experiences several deleterious effects caused by random variations in the refractive index [13]. These negative effects, which include excessive beam spreading, beam wander, angle-of-arrival fluctuations, and scintillation, reduce the reliability of remote sensing systems, laser radar, and free-space optical communications. Thus it is imperative to take action to mitigate or overcome these effects. It has long been appreciated that PCBs are a good choice to reduce the negative effects from turbulence [14]. Many papers have studied strategies to improve turbulence resistance of beams by using different kinds of PCBs, e.g. PCBs with special beam profiles [15], states of polarization [16], phases [17–19], and non-conventional correlation functions [20, 21].

In nearly all the attempts listed above, the beams have a Schell-model degree of coherence, and though they are effective at reducing turbulence effects, this comes with a decrease of intensity in the focal plane. In recent years, however, it was shown that non-uniformly correlated (NUC) beams in turbulence can have, under certain circumstances, not only lower scintillation but higher intensity than GSM beams [22]. Recently, Yu *et al.* looked at the extended class of HNUC beams in turbulence, and demonstrated that the intensity and the scintillation of the beam can be simultaneously optimized in the receiver plane for an appropriate choice of beam order and spatial coherence [12].

The HNUC beams considered previously had circular symmetry. In this paper, we introduce a yet more general class of NUC beams called rectangular Hermite non-uniformly correlated beams, which possess rectangular symmetry and may have their characteristics along the two rectangular axes independently tuned. The propagation properties of such beams are studied in free space and in atmospheric turbulence, and it is shown by that adjusting beam orders and correlation lengths, one can achieve a high constant on-axis intensity over an extended range, and one can control the location of the focal point of RHNUC beams in 3–D space. Furthermore, we investigate the impact of the shift parameter on the beam's resistance to turbulence.

2. Theoretical model for RHNUC beams

The spatial coherence properties of scalar PCBs are characterized by the cross-spectral density (CSD) in the space-frequency domain and by the mutual coherence function in the space-time domain. The CSD is the quantity of choice for studying quasi-monochromatic fields, and it is defined as a two-point correlation function [1],

$$W(\mathbf{r}_1, \mathbf{r}_2) = \langle E^*(\mathbf{r}_1) E(\mathbf{r}_2) \rangle_\omega , \tag{1}$$

where $\mathbf{r}_1$=(x_1, y_1) and $\mathbf{r}_2$=(x_2, y_2) are two arbitrary position vectors transverse to the direction of propagation, $E(\mathbf{r})$ represents the field fluctuating in a direction perpendicular to the z-axis, the asterisk denotes the complex conjugate and the angular brackets $\langle ... \rangle_\omega$ denote an ensemble average over a ensemble of monochromatic field realizations.

The CSD of PCBs can be expressed in the following general form [1],

$$W(\mathbf{r}_1, \mathbf{r}_2) = \sqrt{S(\mathbf{r}_1) S(\mathbf{r}_2)}\, \mu(\mathbf{r}_1, \mathbf{r}_2), \tag{2}$$

where $S(\mathbf{r})$ is the spectral density at point $\mathbf{r}$, and $\mu(\mathbf{r}_1, \mathbf{r}_2)$ is the DOC of the PCB. For HNUC beams with a circularly symmetric DOC, the CSD is defined as [12]

$$W(\mathbf{r}_1, \mathbf{r}_2) = \exp\left(-\frac{\mathbf{r}_1^2 + \mathbf{r}_2^2}{w_0^2}\right) \mu(\mathbf{r}_1, \mathbf{r}_2), \tag{3}$$

with $\mu(\mathbf{r}_1, \mathbf{r}_2)$ given by

$$\mu(\mathbf{r}_1, \mathbf{r}_2) = G_0 H_{2m}\left(\frac{\mathbf{r}_2^2 - \mathbf{r}_1^2}{r_c^2}\right) \exp\left[-\frac{\left(\mathbf{r}_2^2 - \mathbf{r}_1^2\right)^2}{r_c^4}\right], \tag{4}$$

Optics EXPRESS

where w_0 denotes the beam width, r_c is the correlation length, $G_0 = 1/H_{2m}(0)$ and H_{2m} denotes the Hermite polynomial of order $2m$.

Now we introduce the rectangular Hermite non-uniformly correlated beams as a natural extension of circular HNUC beams. The spectral density and the DOC of RHNUC beams in the source plane are given as

$$S(\mathbf{r}) = \exp\left(-\mathbf{r}^2/w_0^2\right), \tag{5}$$

$$\begin{aligned}\mu(\mathbf{r}_1,\mathbf{r}_2) &= \mu_x(x_1,x_2)\,\mu_y(y_1,y_2)\\ &= G_{0x}H_{2m}\left[\frac{(x_1-x_0)^2-(x_2-x_0)^2}{r_{cx}^2}\right]\exp\left[-\frac{\left((x_1-x_0)^2-(x_2-x_0)^2\right)^2}{r_{cx}^4}\right]\\ &\times G_{0y}H_{2n}\left[\frac{(y_1-y_0)^2-(y_2-y_0)^2}{r_{cy}^2}\right]\exp\left[-\frac{\left((y_1-y_0)^2-(y_2-y_0)^2\right)^2}{r_{cy}^4}\right],\end{aligned} \tag{6}$$

where r_{cx} and r_{cy} are the correlation lengths in the x and y directions, respectively, G_{0x}=$1/H_{2m}(0)$ and G_{0y}=$H_{2n}(0)$, x_0 and y_0 are the shift parameters in x and y directions.

To be a mathematically genuine or physically realizable correlation function, the CSD of PCBs must be Hermitian and satisfy the condition of non-negative definiteness. From the definition, it is obvious that it is Hermitian. The condition for non-negative definiteness will be satisfied if it may be written in the form [1],

$$W(\mathbf{r}_1,\mathbf{r}_2) = \int I(\mathbf{v})\,V_0^*(\mathbf{r}_1,\mathbf{v})\,V_0(\mathbf{r}_2,\mathbf{v})\,d^2\mathbf{v}, \tag{7}$$

where V_0 is an arbitrary kernel but I must be a non-negative function. Equation (7) can be expressed in the following alternative form [23],

$$W(\mathbf{r}_1,\mathbf{r}_2) = \iint W_i(\mathbf{v}_1,\mathbf{v}_2)\,V_0^*(\mathbf{r}_1,\mathbf{v}_1)\,V_0(\mathbf{r}_2,\mathbf{v}_2)\,d^2\mathbf{v}_1 d^2\mathbf{v}_2, \tag{8}$$

where

$$W_i(\mathbf{v}_1,\mathbf{v}_2) = \sqrt{I(\mathbf{v}_1)\,I(\mathbf{v}_2)}\,\delta(\mathbf{v}_1,\mathbf{v}_2), \tag{9}$$

here, δ denotes the Dirac delta function. From Eqs. (8) and (9), we see that PCBs with special DOC can be generated from an incoherent source with CSD function $W_i(\mathbf{v}_1,\mathbf{v}_2)$ through propagation by choosing suitable expressions of I and V_0. In such a case, V_0 would be the kernel of a linear optical system.

To generate RHNUC beams, we set I and V_0 as follows:

$$I(\mathbf{v}) = (4\pi)^{-1}\left(\frac{2}{a}\right)^{2m+1}\left(\frac{2}{b}\right)^{2n+1} v_x^{2m}v_y^{2n}\exp\left(-\frac{v_x^2}{a^2}-\frac{v_y^2}{b^2}\right), \tag{10}$$

$$V_0(\mathbf{r},\mathbf{v}) = \exp\left(-\frac{\mathbf{r}^2}{w_0^2}\right)\exp\left[-ikv_x(x-x_0)^2 - ikv_y(y-y_0)^2\right], \tag{11}$$

where $a = 2/kr_{cx}^2$ and $b = 2/kr_{cy}^2$, $k = 2\pi/\lambda$ is the wavenumber. After substituting Eqs. (10) and (11) into Eq. (8), it reduces (after some operations) to the CSD of RHNUC beams. So this CSD satisfies the condition of non-negative definiteness and it is therefore physically realizable. How to realize the system of Eq. (11), however, is an open question.

Optics EXPRESS

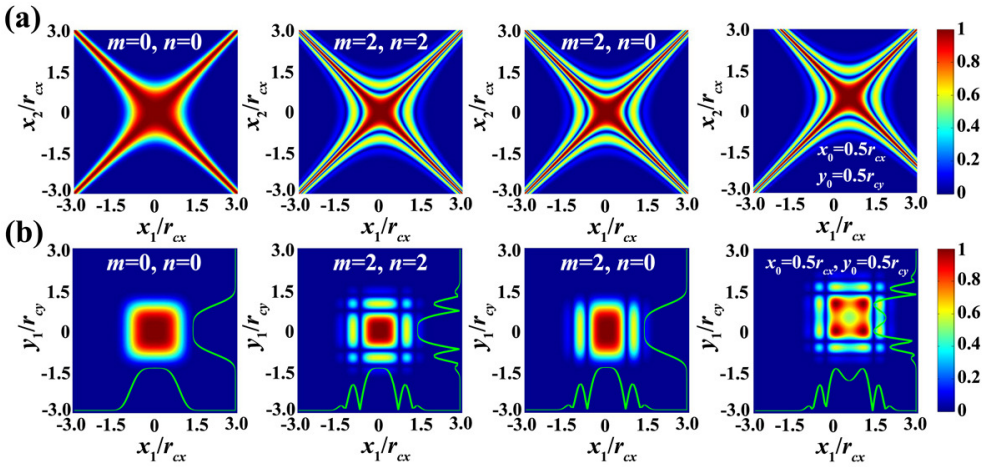

Fig. 1. Density plot of the absolute value of the DOC of RHNUC beams for different beam orders with x_0=y_0=0 and different shift parameters with $m = n = 2$ (a) in the $x_1 - x_2$ plane with $y_1 = y_2 = 0$ (b) in the $x_1 - y_1$ plane with $x_2 = y_2 = 0$.

Figure 1 shows the density plot of the absolute value of the DOC of RHNUC beams for different beam orders and shift parameters in the source plane. One finds that the distribution of the DOC of RHNUC beams in the $x_1 - x_2$ plane is similar to that of the circular HNUC beams mentioned in [12]; however, the distribution of the DOC in the $x_1 - y_1$ plane has rectangular symmetry. The number of side lobes in x and y directions increases as the value of the beam orders m and n increase, respectively. The DOC of RHNUC beams is also dependent on the shift parameters, and the center position is determined by the shift parameters. We therefore have a class of rectangular non-uniformly correlated beams with distinct correlation functions.

3. Cross-spectral density of RHNUC beams propagating in turbulent atmosphere

In general, paraxial propagation of the CSD of PCBs from the source plane $z = 0$ into an arbitrary plane $z > 0$ in free space or a turbulent medium can be treated by the generalized Huygens-Fresnel integral [13],

$$W(\boldsymbol{\rho}_1, \boldsymbol{\rho}_2, z) = \left(\frac{k}{2\pi z}\right)^2 \iint_{-\infty}^{\infty} W_0(\mathbf{r}_1, \mathbf{r}_2) \exp\left[-\frac{ik}{2z}(\mathbf{r}_1 - \boldsymbol{\rho}_1)^2 + \frac{ik}{2z}(\mathbf{r}_2 - \boldsymbol{\rho}_2)^2\right] \times \langle \exp[\Psi(\mathbf{r}_1, \boldsymbol{\rho}_1) + \Psi^*(\mathbf{r}_2, \boldsymbol{\rho}_2)]\rangle \, d^2\mathbf{r}_1 d^2\mathbf{r}_2, \tag{12}$$

where $\boldsymbol{\rho}_1$ and $\boldsymbol{\rho}_2$ represent two arbitrary spatial positions in the receiving plane, $W_0(\mathbf{r}_1, \mathbf{r}_2)$ denotes the CSD of the beams in the source plane, and $\Psi(\mathbf{r}, \boldsymbol{\rho})$ denotes the complex phase perturbation induced by the refractive-index fluctuations of the random medium between $\mathbf{r}$ and $\boldsymbol{\rho}$. In free space, $\Psi(\mathbf{r}, \boldsymbol{\rho}) = 0$. The ensemble average term in Eq. (12) can be expressed as [12],

$$\langle \exp[\Psi(\mathbf{r}_1, \boldsymbol{\rho}_1) + \Psi^*(\mathbf{r}_2, \boldsymbol{\rho}_2)]\rangle = \exp\left\{-\left(\frac{\pi^2 k^2 z}{3}\right)\left[(\boldsymbol{\rho}_1 - \boldsymbol{\rho}_2)^2 + (\boldsymbol{\rho}_1 - \boldsymbol{\rho}_2)\cdot(\mathbf{r}_1 - \mathbf{r}_2) + (\mathbf{r}_1 - \mathbf{r}_2)^2\right]\int_0^{\infty} \boldsymbol{\kappa}^3 \Phi_n(\boldsymbol{\kappa}) \, d^2\boldsymbol{\kappa}\right\}, \tag{13}$$

where $\Phi_n(\boldsymbol{\kappa})$ is the spatial power spectrum of the refractive-index fluctuations of the turbulent atmosphere. For brevity, we set

$$T = \int_0^{\infty} \boldsymbol{\kappa}^3 \Phi_n(\boldsymbol{\kappa}) \, d^2\boldsymbol{\kappa}. \tag{14}$$

Optics EXPRESS

Here, we choose the van Karman power spectrum as the turbulence model, which can account for non-Kolmogorov as well as Kolmogorov ($\alpha = 11/3$) turbulence with inner and outer scales [24, 25]

$$\Phi_n(\boldsymbol{\kappa}) = A(\alpha) C_n^2 \left(\kappa^2 + \kappa_0^2\right)^{-\alpha/2} \exp\left(-\kappa^2/\kappa_m^2\right), \tag{15}$$

where C_n^2 is a generalized refractive-index structure parameter with units $m^{3-\alpha}$, $\kappa_0 = 2\pi/L_0$, with L_0 being the outer scale of turbulence, $\kappa_m = c(\alpha)/l_0$, with l_0 being the inner scale of turbulence, and

$$A(\alpha) = \frac{1}{4\pi^2}\Gamma(\alpha-1)\cos(\alpha\pi/2), c(\alpha) = \left[\frac{2\pi A(\alpha)}{3}\Gamma(5-\alpha/2)\right]^{1/(\alpha-5)}, \tag{16}$$

where $\Gamma(\cdot)$ represents the Gamma function.

With this spectrum, T can be expressed in the following form

$$T = \frac{A(\alpha)}{2(\alpha-2)} C_n^2 \left[\beta\kappa_m^{2-\alpha}\exp\left(\kappa_0^2/\kappa_m^2\right)\Gamma_1\left(2-\alpha/2, \kappa_0^2/\kappa_m^2\right) - 2\kappa_0^{4-\alpha}\right], 3 < \alpha < 4, \tag{17}$$

where $\beta = 2\kappa_0^2 - 2\kappa_m^2 + \alpha\kappa_m^2$ and Γ_1 is the incomplete Gamma function. T is therefore a constant for a given state of turbulence.

Now, we may calculate the CSD of RHNUC beams in the target plane using the above equations. As it is too hard to integrate directly by inserting Eqs. (5) and (6) into Eq. (12), we substitute Eq. (7) into Eq. (12), and after interchanging the orders of the integrals, we obtain the formula

$$W(\boldsymbol{\rho}_1, \boldsymbol{\rho}_2, z) = \int I(\mathbf{v}) P(\boldsymbol{\rho}_1, \boldsymbol{\rho}_2, \mathbf{v}, z)\, d^2\mathbf{v}, \tag{18}$$

where we define $P(\boldsymbol{\rho}_1, \boldsymbol{\rho}_2, \mathbf{v}, z)$ as

$$P(\boldsymbol{\rho}_1, \boldsymbol{\rho}_2, \mathbf{v}, z) = \left(\frac{k}{2\pi z}\right)^2 \iint_{-\infty}^{\infty} V_0^*(\mathbf{r}_1, \mathbf{v}) V_0(\mathbf{r}_2, \mathbf{v}) \exp\left[-\frac{ik}{2z}(\mathbf{r}_1 - \boldsymbol{\rho}_1)^2 + \frac{ik}{2z}(\mathbf{r}_2 - \boldsymbol{\rho}_2)^2\right]$$
$$\exp\left\{-\frac{\pi^2 k^2 z T}{3}\left[(\boldsymbol{\rho}_1 - \boldsymbol{\rho}_2)^2 + (\boldsymbol{\rho}_1 - \boldsymbol{\rho}_2)\cdot(\mathbf{r}_1 - \mathbf{r}_2) + (\mathbf{r}_1 - \mathbf{r}_2)^2\right]\right\} d^2\mathbf{r}_1 d^2\mathbf{r}_2. \tag{19}$$

Substituting from Eq. (11) into Eq. (19), after a lengthy integral calculation, one obtains

$$P(\boldsymbol{\rho}_1, \boldsymbol{\rho}_2, \mathbf{v}, z) = \exp\left[-\frac{ik}{2z}\left(\boldsymbol{\rho}_1^2 - \boldsymbol{\rho}_2^2\right)\right] \exp\left[-\left(\frac{w_0^2 k^2}{8z^2} + \frac{1}{3}\pi^2 k^2 z T\right)(\boldsymbol{\rho}_1 - \boldsymbol{\rho}_2)^2\right] \frac{w_0^2}{2 w_{zx} w_{zy}}$$
$$\times \exp\left\{-\frac{1}{w_{zx}}\left|-i\left[\frac{k w_0^2}{4z}(1 - 2v_x z) - \frac{1}{3}\pi^2 k z^2 T\right](\boldsymbol{\rho}_{1x} - \boldsymbol{\rho}_{2x}) + \left(\frac{\boldsymbol{\rho}_{1x} + \boldsymbol{\rho}_{2x}}{2}\right) - 2 z v_x x_0\right|^2\right\}$$
$$\times \exp\left\{-\frac{1}{w_{zy}}\left|-i\left[\frac{k w_0^2}{4z}(1 - 2v_y z) - \frac{1}{3}\pi^2 k z^2 T\right](\boldsymbol{\rho}_{1y} - \boldsymbol{\rho}_{2y}) + \left(\frac{\boldsymbol{\rho}_{1y} + \boldsymbol{\rho}_{2y}}{2}\right) - 2 z v_y y_0\right|^2\right\}, \tag{20}$$

where

$$w_{zx}^2 = \frac{w_0^2}{2}(1 - 2v_x z)^2 + \left(\frac{\sqrt{2} z}{k w_0}\right)^2 + \frac{4\pi^2 z^3}{3} T, \tag{21}$$

$$w_{zy}^2 = \frac{w_0^2}{2}(1 - 2v_y z)^2 + \left(\frac{\sqrt{2} z}{k w_0}\right)^2 + \frac{4\pi^2 z^3}{3} T. \tag{22}$$

Optics EXPRESS

We obtain the CSD of RHNUC beams after propagation by evaluation of Eq. (18).
The spectral intensity of RHNUC beams in the output plane is defined as

$$S(\boldsymbol{\rho}, z) = W(\boldsymbol{\rho}, \boldsymbol{\rho}, z). \tag{23}$$

The spectral degree of coherence of HNUC beams in the output plane is obtained from the expression

$$\mu(\boldsymbol{\rho}_1, \boldsymbol{\rho}_2, z) = \frac{W(\boldsymbol{\rho}_1, \boldsymbol{\rho}_2, z)}{\sqrt{W(\boldsymbol{\rho}_1, \boldsymbol{\rho}_1, z) W(\boldsymbol{\rho}_2, \boldsymbol{\rho}_2, z)}}. \tag{24}$$

Applying Eqs. (10) and (20)–(24), one can numerically study the evolution properties of the spectral intensity and spectral DOC in free space and in turbulence in a straightforward manner.

4. Numerical calculation results and analysis of propagation properties of RHNUC beams in free space

In this section, we study the propagation properties of RHNUC beams propagating in free space by using the formulas derived above (when $C_n^2 = 0$). In the following examples, the parameters of the beam are set as $\lambda = 632.8$ nm, $w_0 = 5$ cm.

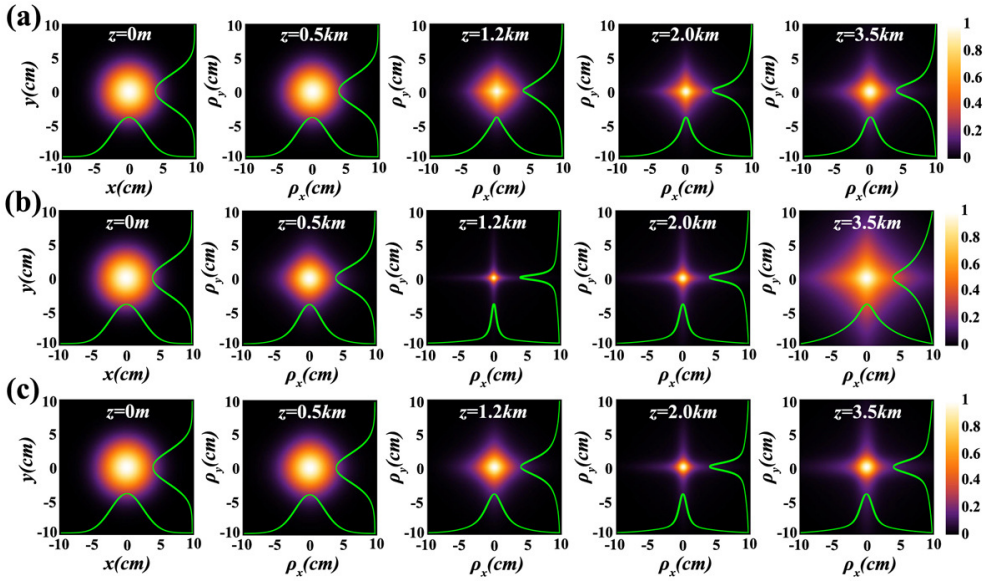

Fig. 2. The normalized intensity of RHNUC beams at different distances for different values of the beam orders and the correlation lengths with no shifting (a) $m = n = 0$, $r_{cx} = r_{cy} = 3$ cm (b) $m = n = 2$, $r_{cx} = r_{cy} = 3$ cm (c) $m = n = 2$, $r_{cx} = r_{cy} = 4$ cm.

Figure 2 shows the intensity for identical orders and correlation lengths along x and y. One observes that the size of the beam spot of RHNUC beams decreases with increasing propagation distance over short ranges, while at long ranges, the spot size increases, which means RHNUC beams possess a self-focusing property, which is similar to the behavior of circular HNUC beams discussed in [12]. However, the distribution of the intensity of RHNUC beams satisfies a Gaussian distribution in the source plane, and it evolves into diamond distribution gradually as the increasing propagation distance. Here, let us define the position of the smallest size, i.e., focal distance, of the beam spot as "Z_f" [e.g., $Z_f = 1.2$ km in Fig. 2(b)]. There is a detailed calculation process of Z_f in Ref. [26]. Comparing with Figs. 2(a) and 2(b), we find that, with increasing

Optics EXPRESS

beam order, the self-focusing property becomes more dramatic and Z_f becomes smaller, but the spot size increases more rapidly at long ranges. We find from Figs. 2(b) and 2(c) that the correlation length also affects the self-focusing property. With a small value of correlation length, the self-focusing property becomes more dramatic and Z_f becomes smaller; the explanation of this is similar to that given in Ref. [12].

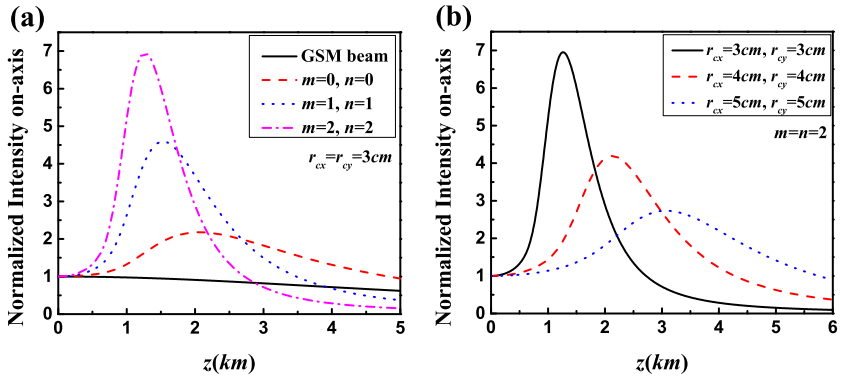

Fig. 3. Normalized intensity on-axis of RHNUC beams propagation in free space (a) with $r_{cx} = r_{cy} = 3$ cm for different beam orders (b) with $m = n = 2$ for different correlation lengths.

Figure 3 shows the normalized intensity on-axis of RHNUC beams in free space for different beam orders and different correlation lengths. One confirms that the on-axis intensity of RHNUC beams increases over short propagation distances to a maximum, after which it decreases gradually. Furthermore, the peak value of the intensity is larger and the Z_f is smaller with increasing beam orders or decreasing correlation lengths, which means the self-focusing property of RHNUC beams with large beam orders or low correlation lengths is more dramatic and both mode orders and correlation lengths may be changed to adjust the focal distance (i.e., the position in z-direction).

In the case of equal mode orders and correlations along x and y, the beam effectively has a point focus and a high intensity over a relatively short propagation range. If different coherence properties are used along x and y, the focusing will be astigmatic; under such a circumstance, an appropriate choice of mode orders and correlation lengths can result in a high constant intensity over an extended propagation range, as we now show.

Figure 4 shows the density plot of the normalized intensity of RHNUC beams propagation at several propagation distances for astigmatic cases ($m \neq n$ and/or $r_{cx} \neq r_{cy}$). We find that the beam spot becomes a squashed diamond distribution at Z_f; over long ranges, the beam profile is also a squashed diamond but is perpendicular to that at Z_f. This phenomenon can be explained by the different focal lengths along x and y for different mode orders or correlation lengths.

Figure 5 shows the focal distance and normalized intensity maximum in x and y directions of RHNUC beams versus the correlation lengths for different beam orders (the results in x and y direction are the same). We find from Fig. 5(a) that the focal distance increases gradually over low coherence to a maximum, after which it decreases rapidly to zero, which indicates that self-focusing disappears with high coherence. Furthermore, the focal distance maximum increases with larger beam orders. Figure 5(b) shows us that the value of normalized intensity maximum of the beam is almost constant for low coherence, and then decreases rapidly with increasing coherence to a value of unity. It should be pointed out that the value of the normalized intensity maximum is 1 for an incoherent beam, which isn't shown in Fig. 5(b). Figure 5 demonstrates lots of flexibility in placing the x and y focal points. According to these observations, we can choose

Optics EXPRESS

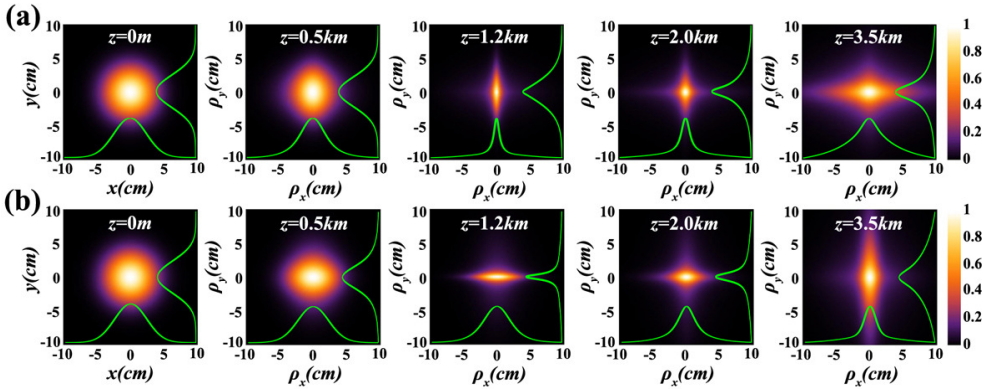

Fig. 4. The astigmatic normalized intensity of RHNUC beams at different distances for different values of the beam orders and the correlation lengths with no shifting (a)m = 2, n = 0, r_{cx} = r_{cy} = 3 cm (b) m = n = 2, r_{cx} = 5 cm, r_{cy} = 3 cm.

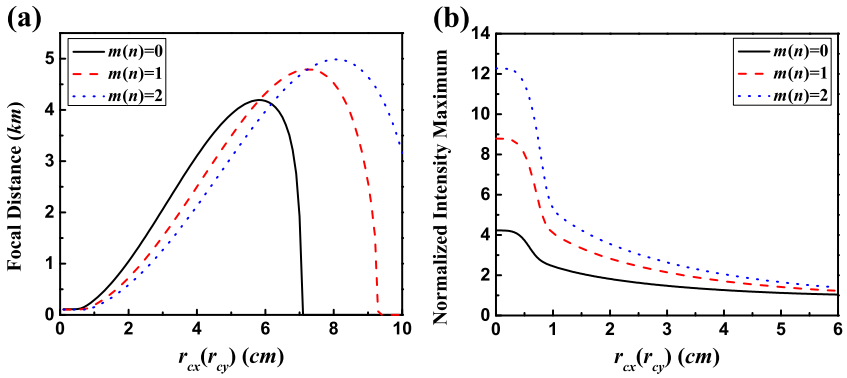

Fig. 5. (a) Focal distance (b) Normalized intensity maximum in $x(y)$ direction of RHNUC beams versus the correlation lengths for different beam orders.

different focal distances and normalized intensity maximums of the beam in x and y directions to realize a flat-topped high intensity profile with respect to propagation distance.

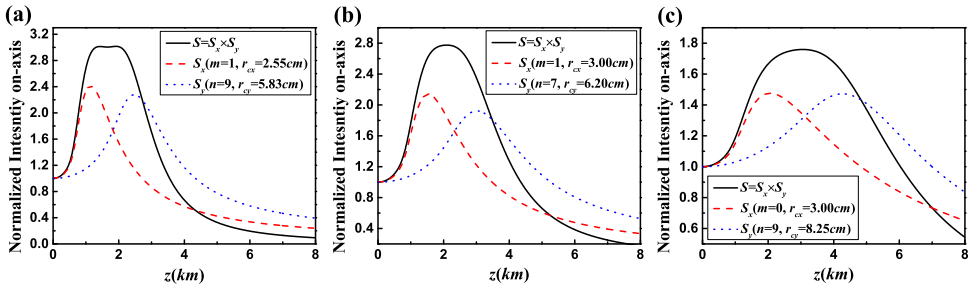

Fig. 6. Normalized intensity of astigmatic RHNUC beams propagation in free space for different beam orders and correlation lengths. S_x and S_y are the normalized intensities in x and y directions, respectively.

Figure 6 shows examples of such flat-topped intensity for different beam orders and correlation

Optics EXPRESS

lengths. One finds that an appropriate choice of mode orders and correlation lengths can achieve flat-topped on-axis intensity over a range on order of a kilometer. Furthermore, we can adjust the beam orders and correlation lengths to control the magnitude and location of the flat-topped intensity. Here, though we present only three results, users can use Fig. 5 to determine for themselves which beam orders and correlation lengths provide optimal results for their application.

5. Numerical calculation results and analysis of propagation properties of RHNUC beams in turbulent atmosphere

In this section, we study the propagation properties of RHNUC beams propagating in turbulence. In the following numerical examples, the parameters of the turbulence are set as $L_0 = 1$ m, $l_0 = 1$ mm, $\alpha = 11/3$ and $C_n^2 = 4 \times 10^{-15}$ m$^{-2/3}$. The Rytov variance $\sigma_1^2 = 1.23 C_n^2 k^{7/6} z^{11/6}$, which represents the scintillation of a plane wave under weak fluctuation conditions, is often used as a rough measure of turbulence strength. For our conditions, $\sigma_1^2 = 1.7$ at 3 km, which indicates strong turbulence.

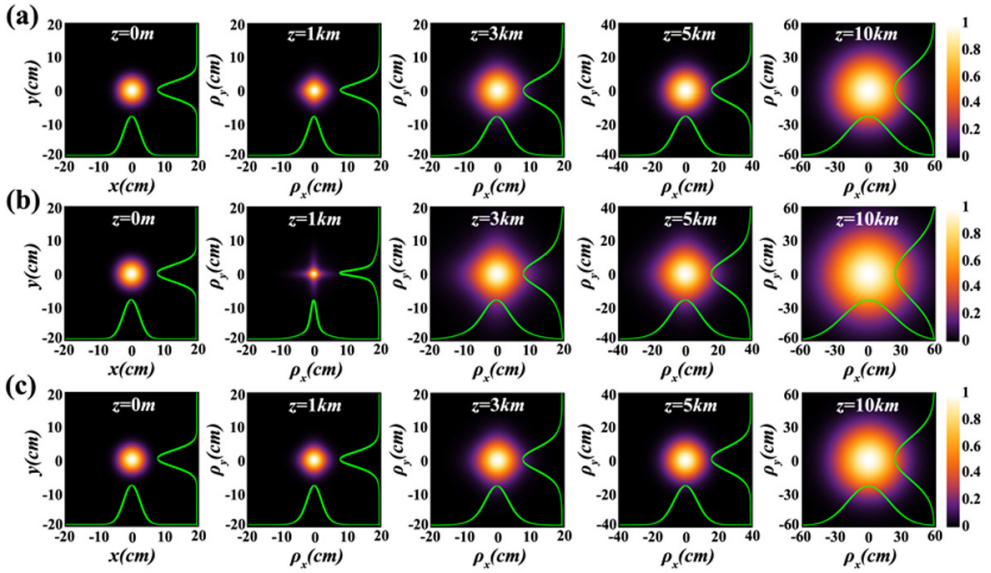

Fig. 7. The normalized intensity of RHNUC beams at different distances in turbulence for different beam parameters with no shifting (a) $m = n = 0$, $r_{cx} = r_{cy} = 3$ cm (b) $m = n = 2$, $r_{cx} = r_{cy} = 3$ cm (c) $m = n = 2$, $r_{cx} = r_{cy} = 4$ cm.

Figure 7 shows the normalized intensity of RHNUC beams at different distances in turbulence with different beam orders and correlation lengths. We confirm that the self-focusing property of such beams still works in turbulence. Figure 7 shows that the intensity profile of RHNUC beams evolves from a Gaussian profile in the source plane, to a diamond distribution in the self-focusing plane (similar to the free-space case), to a Gaussian profile again at a long propagation distance. One can explain this phenomenon by the fact that the influence of turbulence can be neglected and the free-space diffraction plays a dominant role at short propagation distance, thus the propagation properties of RHNUC beams in turbulence is similar to those in free space. With the further increase of the propagation distance, the influence of turbulence accumulates and plays a dominant role gradually, and the diamond distribution beam profile evolves into Gaussian distribution beam profile at long distance due to the isotropic influence of turbulence.

Optics EXPRESS

Comparing with Figs. 7(a) and 7(b), one finds that the evolution properties of the intensity are closely related to the beam orders m and n, the conversion from the diamond distribution to Gaussian distribution becomes slower as the beam orders m and n increase, which means that RHNUC beams with large m and n are less affect by turbulence. We confirm from Figs. 7(b) and 7(c) that RHNUC beams with low correlation lengths can keep the diamond distribution beam profile longer propagation distance than RHNUC beams with high correlation lengths, which means that RHNUC beams with low correlation lengths are less affected by turbulence.

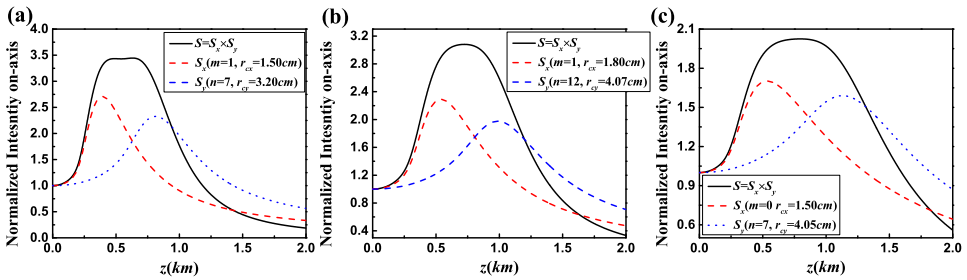

Fig. 8. Normalized intensity of astigmatic RHNUC beams propagation in turbulence for different beam orders and correlation lengths. S_x and S_y are the normalized intensities in x and y directions, respectively.

Figure 8 shows the flat-topped intensity of RHNUC beams propagation in turbulence for different beam orders and correlation lengths. One confirms from Fig. 8 that one can also choose an appropriate mode orders and correlation lengths to achieve flat-topped on-axis intensity in turbulence. For applications, this flat-topped profile could reduce sensitivity to range errors.

Figure 9 shows the density plot of the absolute value of the DOC of RHNUC beams for different beam orders and correlation lengths in free space and turbulence. We find from Fig. 9 that the spectral DOC of RHNUC beams displays a rectangular symmetry array distribution (if $m = n = 0$, just like a rectangle) in the source plane, evolves into a different array distribution at short distance and then regains the profile similar to that in the source plane in free space [see Fig. 9(a)]. In turbulence, however, the rectangular symmetry distribution of DOC gradually disappears on propagation and the spectral DOC finally becomes of Gaussian distribution in the far field. Furthermore, the evolution properties of the DOC are closely related to the beam orders [see Figs. 9(b) and 9(c)] and also related to the correlation lengths [see Figs. 9(b) and 9(d)]. We find that the conversion from the array distribution to Gaussian distribution becomes slower as the beam orders m and n increase or the correlation lengths decrease in turbulence, which means that RHNUC beams with large beam orders or low correlation lengths are less affected by turbulence from the perspective of the spectral degree of coherence.

We therefore conclude that the self-focusing property of RHNUC beams also works and flat-topped and high intensity also can be realized in turbulent atmosphere. Furthermore, RHNUC beams with large beam orders and low coherence are less affected by the turbulence.

6. Numerical calculation results and analysis of effect of the shift parameters on propagation properties of RHNUC beams

The shift property of RHNUC beams allows their transverse position to be adjusted at the detector by adjusting the source statistics alone. Figure 10(a) shows the normalized intensity of RHNUC beams on propagation in free space at several propagation distances with given shift parameters ($x_0 = y_0 = 2$ cm) and Fig. 10(b) shows the normalized intensity of RHNUC beams at the focal plane $Z_f = 1.2$ km for different values of the shift parameters.

These results show clearly that we can control the location of the beam center (intensity

Optics EXPRESS

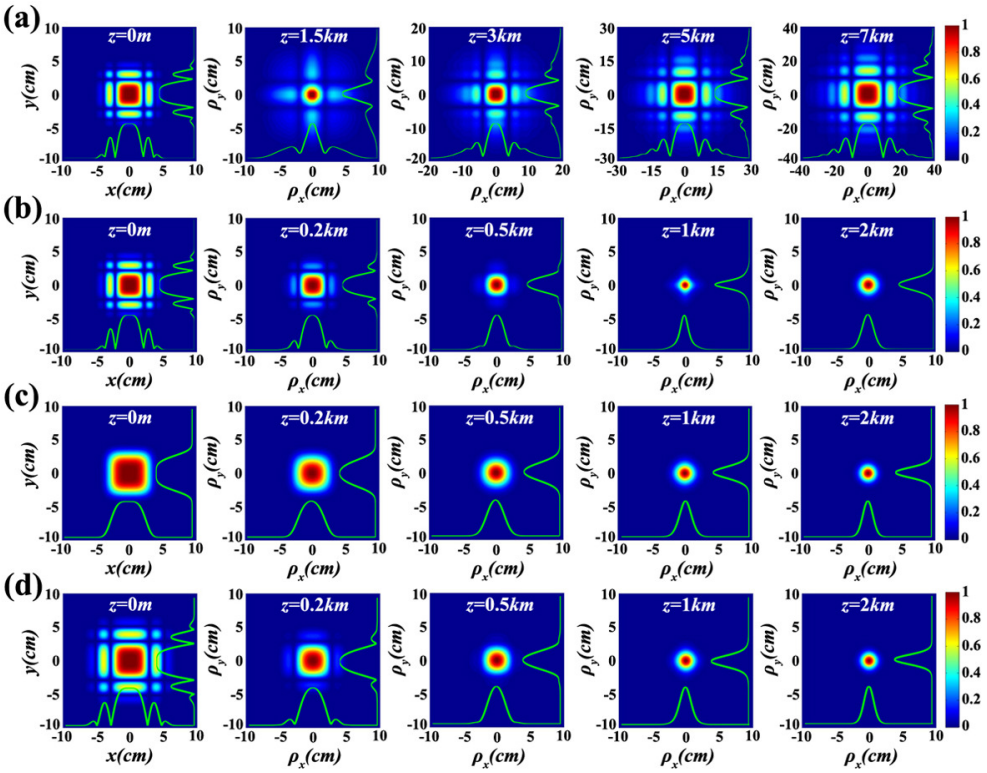

Fig. 9. Density plot of the absolute value of the DOC of RHNUC beams for different beam orders and correlation lengths with no shifting in free space (a) $m = n = 2$, $r_{cx} = r_{cy} = 3$ cm; and in turbulence (b) $m = n = 2$, $r_{cx} = r_{cy} = 3$ cm (c) $m = n = 0$, $r_{cx} = r_{cy} = 3$ cm (d) $m = n = 2$, $r_{cx} = r_{cy} = 4$ cm.

maximum) in receive plane (i.e., $x - y$ plane) by adjusting the shift parameters. Hence, together with the earlier discussion of focal control, we find that one can control the location of the focus point in full 3–D space by adjusting the initial parameters of RHNUC beams.

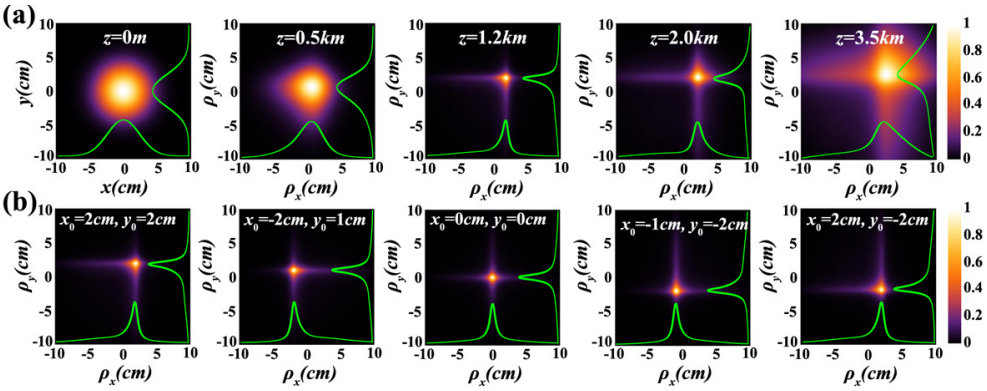

Fig. 10. The normalized intensity of RHNUC beams in free space with $m = n = 2$, $r_{cx} = r_{cy} = 3$ cm (a) at several propagation distances with $x_0 = y_0 = 2$ cm; (b) with different values of the shift parameters at $z = 1.2$ km.

Optics EXPRESS

It should be noted that turbulence will degrade the shifting behavior. Figure 11 shows that shift distance (SD) of the intensity maximum of the beam versus the propagation distance in free space and in turbulence and degradation rate (η) of shift distance of the intensity maximum of the beam in turbulence with different shift parameters. Here, we defined the SD and the degradation rate as follows,

$$SD = \sqrt{\rho_x^2 + \rho_y^2}, \tag{25}$$

$$\eta = \frac{|SD_t - SD_f|}{SD_f} \times 100\%, \tag{26}$$

where (ρ_x, ρ_y) denotes the position coordinate of the intensity maximum of the beam spot, SD_f and SD_t denote the shift distance of the intensity maximum of the beam spot in free space and in turbulence, respectively.

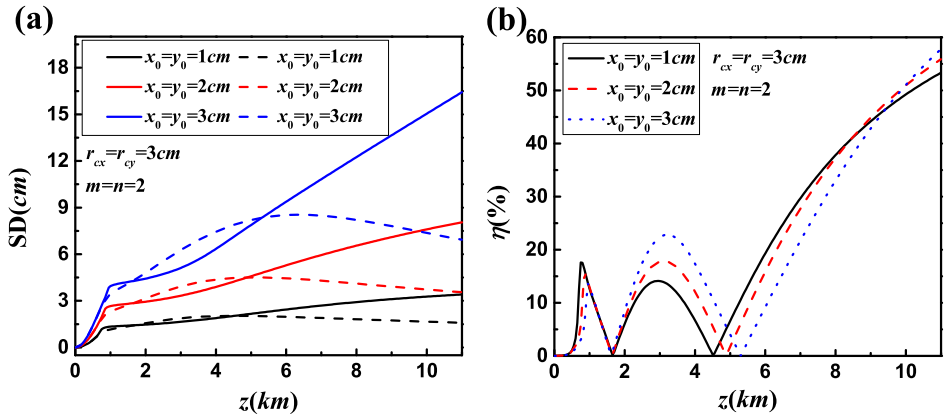

Fig. 11. (a) Shift distance of the intensity maximum of RHNUC beams versus the propagation distance in free space (solid line) and in turbulence (dash line); and (b) degradation rate of shift distance of the intensity maximum of the beam in turbulence with different shift parameters.

We find from Fig. 11(a) that the SD increases rapidly at short propagation distance, while at long distance, it increases gradually in free space. However, in a turbulent atmosphere the SD increases to a maximum, after which it decreases asymptotically to a fixed value, which implies that the shifted beam spot returns to a Gaussian beam profile, gradually, due to the influence of the turbulence. One confirms from Fig. 11(b) that, at a short distance (i.e., $z < 1$ km) and the propagation distance between about 5.5 km $\leq z \leq$ 9 km, the degradation rate decreases with the increasing beam shift parameters, which means RHNUC beams can better to keep the original transmission path with large shift parameters, i.e., we can also adjust the shift parameters of RHNUC beams to optimize effects for a given propagation distance.

7. Summary

We have studied the propagation of RHNUC beams in free space and in turbulence. Analytical expressions for the CSD of RHNUC beams in turbulence have been derived and the evolution properties of the spectral intensity, and the spectral DOC of such beams have been illustrated numerically. We have found that adjusting the beam orders and correlation lengths can realize flat-topped astigmatic intensity profiles, and one can adjust the initial beam parameters of RHNUC beams to control the focus point in 3D space. Furthermore, adjusting the beam orders and the correlation lengths of the beam can mitigate negative effects from turbulence. Moreover, we

Optics EXPRESS

can also adjust the shift parameters of RHNUC beams to optimize effects for given propagation distance between a signal transmitter and receiver.

Funding

National Natural Science Fund for Distinguished Young Scholar (11525418); National Natural Science Foundation of China (NSFC) (91750201); Project of the Priority Academic Program Development of Jiangsu Higher Education Institutions; China Scholarship Council (CSC) (201706920103).

References

1. L. Mandel and E. Wolf, *Optical Coherence and Quantum Optics* (Cambridge University, 1995).
2. G. Gbur and T. D. Visser, "Can spatial coherence effects produce a local minimum of intensity at focus," Opt. Lett. **28**(18), 1627–1629 (2003).
3. S. A. Ponomarenko, "A class of partially coherent beams carrying optical vortices," J. Opt. Soc. Am. A **18**(1), 150-156 (2001).
4. F. Gori and M. Santarsiero, "Devising genuine spatial correlation functions," Opt. Lett. **32**(24), 3531–3533 (2007).
5. F. Gori, V. R. Sánchez, M. Santarsiero, and T. Shirai, "On genuine cross-spectral density matrices," J. Opt. A: Pure Appl. Opt. **11**(8), 085706 (2009).
6. S. Sahin and O. Korotkova, "Light sources generating far fields with tunable flat profiles," Opt. Lett. **37**(14), 2970–2972 (2012).
7. Z. Mei and O. Korotkova, "Random sources generating ring-shaped beams," Opt. Lett. **38**(2), 91–93 (2013).
8. Y. Chen, J. Gu, F. Wang, and Y. Cai, "Self-splitting properties of a Hermite-Gaussian correlated Schell-model beam," Phys. Rev. A **91**(1), 013823 (2015).
9. L. Ma and S. A. Ponomarenko, "Free-space propagation of optical coherence lattices and periodicity reciprocity," Opt. Express **23**(2), 1848–1856 (2015).
10. H. Lajunen and T. Saastamoinen, "Propagation characteristics of partially coherent beams with spatially varying correlations," Opt. Lett. **36**(20), 4104–4106 (2011).
11. D. Wu, F. Wang, and Y. Cai, "High-order nonuniformly correlated beams," Opt. Laser Technol. **99**, 230–237 (2018).
12. J. Yu, F. Wang, L. Liu, Y. Cai, and G. Gbur, "Propagation properties of Hermite non-uniformly correlated beams in turbulence," Opt. Express **26**(13), 16333–16343 (2018).
13. L. C. Andrews and R. L. Phillips, *Laser Beam Propagation through Random Media* (SPIE, 2005).
14. G. Gbur, "Partially coherent beam propagation in atmospheric turbulence," J. Opt. Soc. Am. A **31**(9), 2038–2045 (2014).
15. Y. Huang, A. Zeng, Z. Gao, and B. Zhang, "Beam wander of partially coherent array beams through non-Kolmogorov turbulence," Opt. Lett. **40**(8), 1619–1622 (2015).
16. F. Wang, X. Liu, L. Liu, Y. Yuan, and Y. Cai, "Experimental study of the scintillation index of a radially polarized beam with controllable spatial coherence," Appl. Phys. Lett. **103**(9), 091102 (2013).
17. F. Wang, Y. Cai, H. T. Eyyuboğlu, and Y. Baykal, "Twist phase induced reduction in scintillation of a partially coherent beam in turbulent atmosphere," Opt. Lett. **37**(2), 184–186 (2012).
18. X. Liu, Y. Shen, L. Liu, F. Wang, and Y. Cai, "Experimental demonstration of vortex phase-induced reduction in scintillation of a partially coherent beam," Opt. Lett. **38**(24), 5323–5326 (2013).
19. J. Wang, H. Wang, S. Zhu, and Z. Li, "Second-order moments of a twisted Gaussian Schell-model beam in anisotropic turbulence," J. Opt. Soc. Am. A **35**(7), 1173–1179 (2018).
20. X. Liu, J. Yu, Y. Cai, and S. A. Ponomarenko, "Propagation of optical coherence lattices in the turbulent atmosphere," Opt. Lett. **41**(18), 4182–4185 (2016).
21. J. Yu, Y. Chen, L. Liu, X. Liu, and Y. Cai, "Splitting and combining properties of an elegant Hermite-Gaussian correlated Schell-model beam in Kolmogorov and non-Kolmogorov turbulence," Opt. Express **23**(10), 13467–13481 (2015).
22. Y. Gu and G. Gbur, "Scintillation of nonuniformly correlated beams in atmospheric turbulence," Opt. Lett. **38**(9), 1395–1397 (2013).
23. F. Wang, X. Liu, Y. Yuan, and Y. Cai, "Experimental generation of partially coherent beams with different complex degrees of coherence," Opt. Lett. **38**(11), 1814–1816 (2013).
24. I. Toselli, L. C. Andrews, R. L. Phillips, and V. Ferrero, "Angle of arrival fluctuations for free space laser beam propagation through non-Kolmogorov turbulence," Proc. SPIE **6551**, 65510E (2007).
25. I. Toselli, L. C. Andrews, R. L. Phillips, and V. Ferrero, "Free-space optical system performance for laser beam propagation through non-Kolmogorov turbulence," Opt. Eng. **47**(2), 026003 (2008).
26. C. Ding, M. Koivurova, J. Turunen, and L. Pan, "Self-focusing of a partially coherent beam with circular coherence," J. Opt. Soc. Am. A **34**(8), 1441–1447 (2017).